LONG RANGE CHANNEL PREDICTION IN AERONAUTICAL TELEMETRY

Marilynn P. Wylie *
Open Door Technologies, LLC
Irving, TX 75063
mwylie@opendoor-technologies.com

ABSTRACT

Long range prediction exploits the principal that the memory span of a predictive filter increases when it samples the input signal at a lower rate. Within the context of a communication system that employs adaptive modulation and coding communication, this implies that by measuring the channel at a rate that is minimally twice the highest Doppler frequency rather than twice the data rate (the latter typically being orders of magnitude greater than the former), one can predict the channel fades much farther ahead into the future.

In this paper, we consider an application of a recursive weighted least squares estimation (WLSE) algorithm to the problem of long range channel prediction. The algorithm is applied to ten sets of channel measurements that have been made during channel sounding exercises on the Edwards Air Force Base test range and include the following scenarios: taxiway, takeoff, in-flight and final approach & landing. In this subset of the measurement campaigns, the test article speed varies from $\approx$ 5 m/s along the taxiway to $\approx$ 100 m/s while in flight. As our results show, the algorithm can be used in real time to predict several milliseconds in the future while using a modest number of filter coefficients ($d = 2$ and $d = 4$ are considered), thus demonstrating that channel prediction is viable in the aeronautical telemetry testing environment.

INTRODUCTION

Under the proposed INET (Integrated Network) architectural vision for future telemetry systems, the research and evaluation community would benefit by an upgrade of the legacy one-way communication system to a bi-directional system that would allow the test directors to communicate with the flight testers. This new communication protocol would potentially decrease the need to repeat as many flight tests due to data corruption, as the ground station control would be able to request a retransmission of corrupted data *during* the flight test. However, the complexity of the aeronautical telemetry channel will impact the fidelity of the data that is measured at the ground station, and this constraint motivates the introduction of adaptive transmission methods, which can potentially aid in the achievement of higher data rates (at the expense of a higher bit rate) by exploiting channel behavior.

In order to realize the full potential of adaptive transmission techniques, the Resource Allocation unit (which would determine the optimal transmission scheme) needs accurate channel state information for the next transmission frame. In many commercial systems, the channel state is estimated at the receiver and then fed back to the transmitter. However, in the highly dynamic environment of flight testing where aeronautical manuevers can be characterized by very high speeds, the rapid channel variations that are caused by multipath fading and the Doppler effect can quickly render the latest channel measurement outdated. Thus, it is advisable to consider the feasibility of long range (in time) channel prediction, and this is the motivation of our study.

Fading channel prediction has long been studied for mobile radio adaptive transmission systems, such as in [1], [2], where critical issues involving complexity, robustness and the design and analysis of transmission adaptation methods have been thoroughly examined. There it is shown that accurate channel prediction can enable adaptive transmission in various applications. The most salient feature of the approach is to demonstrate that by adopting a sampling rate that is much lower than the date rate but on the order of twice the maximum Doppler frequency

*Approved for public release; distribution is unlimited. 412TW-PA-14279.

(which may be a hundred times less than the symbol rate), that the prediction filter can achieve a much higher memory span. Consequently, the channel prediction capability reaches farther ahead in the future. In [3], it is shown that by sampling the at twice the Doppler rate, that the autoregressive filter parameters used to model and predict the channel actually span a much longer time frame than they would if the sample rate was dictated by the data rate. By predicting the future envelope variations, the future fade events are potentially identified so that the appropriate modulation and coding scheme can be applied. Interpolation between predicted values can also be used to improve resolution [4].

Long range channel prediction based on nonstationary parametric modeling has also been explored, as in [5] where the use of nonstationary multicomponent polynomial phase signals is proposed. By exploring an iterative and recursive method for detecting the number of signals and the order of the polynomial phase terms, [5] demonstrates how to predict the channel L steps ahead in time, taking into account the accuracy in detection in the number of signal components and how the accuracy degrades when using iterative procedures are applied.

The contribution of this paper is to apply the long range prediction approach to actual channel measurements that have been acquired on a test range (see [6] for a comprehensive description of the measurement set up) during various testing scenarios which include taxiway, take-off, en-route and final approach & landing. Empirical observations suggest that an autogressive model may well apply to the individually fading taps in the wideband profile, and we use this assumption in order to explore the predictive performance of the Weighted Least Squares Estimation WLSE approach under dynamic conditions that range from test article speeds of ≈ 5 m/s to ≈ 100 m/s.

CHANNEL MODEL

Most aeronautical telemetry channels are well modeled as the superposition of M' paths (which may include a line of sight component), each having a time-varying amplitude and delay:

$$c(\tau, t) = \sum_{m=0}^{M'-1} \tilde{c}_m(t)\delta(t - \tilde{\tau}_m(t)) \tag{1}$$

where $\tilde{c}_m(t)$ denotes the complex fading path amplitude of the m^{th} arrival path, $\tilde{\tau}_m(t)$ denotes its arrival time relative to the line of sight path and $\delta(t)$ is the Kronecker delta function. By referential modeling, $\tilde{\tau}_0(t) = 0$ and (after normalizing with respect to the phase of the line of sight component), $\Im\{\tilde{c}_0(t)\} = 0$. (1) is demonstrative of a tapped delay line containing time-varying coefficients. This non-stationary structure can arise when there is relative motion during flight testing as multipath arrivals along the route exhibit an evolutionary birth and death process in response to appearance of new reflecting or scattering sources and the cessation of influence of past reflectors.

In order to facilitate time variation of the path gain during long range channel prediction, we adopt a model that defines the delay axis as having fixed, equi-spaced delays associated with time-varying gains ($\tau_m = m\Delta : m \in \{0, 1, 2, \cdots, \}; \Delta > 0$). The time-varying gain associated with the superposition of paths that falls in the m^{th} bin of the delay axis can be decomposed into its in-phase and quadrature components, respectively:

$$c_m(t) = c_{m,1}(t) + jc_{m,2}(t) = \sum_{n=1}^{2} -j^{n+1} \cdot c_{m,\alpha}(t). \tag{2}$$

The modified channel model, which uses the discretized delay bins and collects the total path energy falling into each bin, is characterized as having N equally spaced taps:

$$\tilde{c}(\tau, t) = \sum_{m=0}^{N-1} c_m(t)u(\tau - \tau_m) \tag{3}$$

where

$$u(\tau) = \begin{cases} 1 & \tau = 0 \\ 0 & \text{else.} \end{cases} \tag{4}$$

In the sequel, we consider techniques for predicting the amplitude of $\{c_{m,\alpha}(t)\}$ for $\alpha = 1, 2$ and $m = 0, \cdots, N-1$ based on past channel observations.

A. Application of an Autoregressive Channel Model

In order to apply the prediction filter to measured channel data, we have to assume a mathematical model that well characterizes the amplitude fluctutations of each tap in the channel. In this section, we discuss the applicaton of an autoregressive model, which constructs a prediction of the tap amplitude at the next measurement instant by using a weighted summation of past channel tap measurements. The calculation of the filter coefficients (i.e., weights), which may be static or dynamically updated based on prediction error, are actually determined by the methodology of the predictive algorithm.

Simply expressed, given d ($d \geq 1$) observations of the (m, α) *th* fading tap in the multipath profile, over short intervals we apply the model:

$$\hat{c}_{m,\alpha}(t) = \sum_{n=1}^{d} a_{m,\alpha}(n,t) c_{m,\alpha}(t - nLT_0) \tag{5}$$

where $L \geq 1$ denotes the prediction horizon, T_0 is the time between consecutive samples of the channel, $\alpha = 1$ corresponds to the in-phase component, $\alpha = 2$ refers to the quadrature component and d denotest the autoregressive filter order. The filter coefficients are represented by the set: $\{a_{m,\alpha}(1,t), \cdots, a_{m,\alpha}(d,t)\}$. It is our objective to produce the *predicted* value: $\hat{c}_{m,\alpha}(t)$. Clearly, by selecting $L > 1$, we are effectively performing L-step ahead prediction (with a LT_0 second window) without having to apply an L-th order recursive filter. Instead, by sampling at a rate that is L times slower $\left(\frac{1}{LT_0}\right)$, a one-steap ahead predictor actually performs the prediction L time steps ahead in the future. Herein lies the distinguishing feature of the long range predicton methodology.

Long Range Channel Prediction Using the Weighted Least Squares Approach

In this section, we discuss how the WLSE method may be used to adaptively update the filter coefficients in (5). Using the WLSE approach [7], we construct a filter that minimizes the root mean squared error between the predicted versus the actual values of the fading tap gains in the measured aeronautical telemetry flight testing channel. This approach is desirable in that it is dynamic and may be performed in *real time* after d initial observations have been made.

Assume that we have d fading tap measurements taken at time epochs that are separated by LT_0 seconds in time (i.e., $t = \{-dLT_0, -(d-1)LT_0, \cdots, -LT_0\}$). We use the WLSE approach in order to predict the tap gain LT_0 seconds ahead (i.e., at time $t = 0$).

The WLS filter input at time $t - LT_0$ is defined as the following vector of measurements:

$$\mathbf{c}_{m,\alpha}(t - LT_0) = \left[\; c_{m,\alpha}(t - LT_0) \quad c_{m,\alpha}(t - 2LT_0) \quad \cdots \quad c_{m,\alpha}(t - dLT_0) \; \right]'. \tag{6}$$

$(\cdot)\prime$ denotes complex conjugate transpose.

The predicted tap amplitude is computed as the inner product of the linear prediction coefficient vector, $\mathbf{a}_{m,\alpha}(t)$, with the channel observation vector, $\mathbf{c}_{m,\alpha}(t - LT_0)$:

$$\hat{c}_{m,\alpha}(t) = \mathbf{a}'_{m,\alpha}(t) \mathbf{c}_{m,\alpha}(t - LT_0) = \sum_{n=1}^{d} a_{m,\alpha}(n,t) \cdot c_{m,\alpha}(t - nLT_0) \tag{7}$$

where the filter time-varying coefficients are defined as:

$$\mathbf{a}_{m,\alpha}(t) = \left[\begin{array}{cccc} a_{m,\alpha}(1,t) & a_{m,\alpha}(2,t) & \cdots & a_{m,\alpha}(d,t) \end{array} \right]'. \tag{8}$$

The WLSE algorithm may be summarized as follows:

- Select the prediction horizon, LT_0, and the filter order, d.
- At time = $t = 0^-$, initialize the algorithm with the $d \times 1$ unit vector $\mathbf{a}_{m,\alpha}(0) = \left[\begin{array}{ccccc} 1 & 0 & 0 & \cdots & 0 \end{array} \right]'$ and the $d \times d$ identity matrix: $\mathbf{P}_{m,\alpha}(0) = \mathbf{I}$.
- Initialize using the past d channel measurements: $\{c_{m,\alpha}(-dLT_0), \cdots, c_{m,\alpha}(-LT_0)\}$.
- Choose a value for the forgetting vactor, β (typically $-0.95 \leq \beta \leq 0.99$).
- For all $t \geq 0^-$ and for each quadrature component, $\alpha \in \{1, 2\}$, do the following:
  1. Calculate the current predicted channel tap: $\hat{c}_{m,\alpha}(t) = \mathbf{a}'_{m,\alpha}(t) c_{m,\alpha}(t - LT_0)$
  2. Update the current coefficient for the upcoming iteration (at time t):

$$\mathbf{a}_{m,\alpha}(t + LT_0) = \mathbf{a}_{m,\alpha}(t) + \left(\frac{\mathbf{P}_{m,\alpha}(t)\mathbf{c}_{m,\alpha}(t - LT_0)}{\beta + \mathbf{c}'_{m,\alpha}(t - LT_0)\mathbf{P}(t)\mathbf{c}_{m,\alpha}(t - LT_0)} \right) \{c_{m,\alpha}(t) - \hat{c}_{m,\alpha}(t)\} \tag{9}$$

  3. Update the covariance matrix $\mathbf{P}_{m,\alpha}(t)$ for the next iteration:

$$\mathbf{P}_{m,\alpha}(t + LT_0) = \frac{1}{\beta} \left\{ \mathbf{P}_{m,\alpha}(t) - \frac{\mathbf{P}_{m,\alpha}(t)\mathbf{c}_{m,\alpha}(t - LT_0)\mathbf{c}'_{m,\alpha}(t - LT_0)\mathbf{P}_{m,\alpha}(t)}{\beta + \mathbf{c}'_{m,\alpha}(t - LT_0)\mathbf{P}_{m,\alpha}(t)\mathbf{c}_{m,\alpha}(t - LT_0)} \right\}. \tag{10}$$

Simulation results

Iin this section, we present the simulation results obtained using the WLSE prediction algorithm. The test channels used in this study, which are summarized in the Table (1), represent a small subset of themeasurements taken during flight maneouevers at Edwards Air Force Base. More details of the channel measurement campaign are specified in [6].

In each case, the (resampled) channel has a total of 207 taps with a tap spacing of $\Delta\tau = (1/20.625)\mu$s. Hence, we observe each channel for 800μs. The interval between consecutive samples of the channel (in time) is 800μs (corresponding to a sample rate of 1250 Hz). The test article speeds during each measurement interval is also indicated.

Figs. (1a) and (1b) provide a visual indication of the predictive performance of the WLS algorithm for the first two taxiway scenarios (Cases 1 and 2). The prediction horizon and filter order are, respectively, $LT_0 = (1 \cdot 0.8)$ ms and $d = 2$ (1.6 ms). This corresponds to one-step ahead prediction using two filter coefficients. In each case, we are comparing the in-phase component of the line of sight tap as a function of time ($c_{0,1}(t)$) to its prediction, $\hat{c}_{0,1}(t)$. As shown, the predictive algorithm is responsive to the autoregressive model, and gives a reliable prediction of the channel fluctuations for this low filter order ($d = 2$). Similar results have been obtained for all of the other active taps in the profile but have been omitted due to space restrictions.

Evaluation of taxiway Cases 1 and 2 is continued in Figs. 2a and 2b. However, in those figures we show a comparison of the behavior of the in-phase channel taps versus the predicted in-phase channel taps for $LT_0 = (4{\cdot}0.8)$ ms and $d = 4$ (3.2 ms predictive window and looking 3.2 ms back in time). As shown, the algorithm is well capable of predicting the fades and gains of the channel 3.2 ms ahead in real time by using a sliding window of

Case	Scenario	Vehicle speed (m/s)
1	Taxiway E (S-N)	5.29
2	Taxiway E (S-N)	5.08
3	Taxiway E (S-N)	6.31
4	Takeoff on 22L	67.59
5	Cords Road (W-E)	107.16
6	Cords Road (W-E)	107.12
7	Black Mountain (W-E)	106.82
8	Black Mountain (W-E)	110.04
9	Final Approach and Landing on 22L	61.78
10	Final Approach and Landing on 22L	22.72

Table 1: Measurement Scenarios at Edwards Air Force Base

past measurements. Similar results have been obtained for the quadrature component of the channel, but have been omitted due to space restrictions.

The same parameters have been used to study performance of the prediction algorithm in the remainder of the channels. In Figs. (3a) and (3b), we compare the predicted in-phase component of the line of sight path to the actual measurement when $L = 1$ and $d = 2$ in the third taxiway and takeoff environments (Cases 3 and 4, respectively). As the results indicate, the algorithm performs well in both cases, even though there is an order of magnitude difference in the test article speed when comparing the taxiway to the takeoff events.

Next, we consider a longer prediction horizon and higher filter order for Cases 3 and 4: ($L = 4$ and $d = 4$). As shown in Figs. (4a) and (4b), the prediction algorithm is able to follow the path fluctuations very well. There is some hyper-activity in the prediction of one of the wekaer paths at around (680 ms) (the curve is in red) which quickly dies out, and this may be due to the sudden emergence of this reflective path in the profile.

The next set of comparative plots are from flight testing above Cords Road (see Figs. (5a) and (5b)). In this case, as before, $L = 1$ and $d = 2$, and the predictive algorithm is able to predict the line of sight path fluctuations. Next, looking at all of the active taps for the same scenarios (but now considering $L = 4$ and $d = 4$), we see in Figs. (6a) and (6b) that the path activity of all of the taps is well predicted using our WLSE approach. Recall that these maneouvers are characterized by the highest test article speeds available in our data set (≈ 100 m/s).

During the flight, when the test article is above Black Mountain (see Figs. (7a) and (7b)), the line of sight component in both cases is predicted well using $L = 1$ and $d = 2$. The ability to predict the faster fluctuations that are present in the measurements of Fig. (7b) demonstrate that the sampling rate selected (1250 Hz) is adequate to capture the rapidly varying amplitude of this path, and that a higher sampling rate (i.e., that would be on the order of the data rate) is not necessary. A comparison of the performance of the algorithm for all taps in the channel is shown in Figs. (8a) and (8b) for $L = 4$ and $d = 4$. Again, the prediction technique is able to perform well in real time during the flight testing.

Finally, the last set of comparative plots is shown in Figs. (9a) and (9b). This refers to the final approach & landing scenario, where the vehicle speed is ≈ 61.78 m/s (top) and the lowered speed of 22.72 m/s (bottom). Obviously, the first scenario generates a faster fluctutating signal, but the prediction algorithm does capture the fading behavior of the line of sight channel tap. The performance of all of the in-phase tap components is compared in Figs. (10a) and (10b), and again demonstrates that the algorithm performs well during this stage of flight testing as well.

Conclusion

In this paper, we have considered the application of long range channel prediction algorithms to channel measurements taken at Edwards Air Force Base during a flight test. The WLSE predictive technique has been explored. Our results indicate that at the low sampling rate of 1250 Hz, that we have adequately sampled the channel in order to predict its fluctuations in various scenarios, including taxiway, takeoff, en-route and final approach & landing. Our results indicate that the WLSE performs well for low filter orders and that faithful prediction of channel behavior is feasible for test article speeds varying between ≈ 5 m/s and ≈ 100 m/s and for a prediction window that is on the order of milliseconds.

ACKNOWLEDGEMENT

This project is funded by the Test Resource Management Center (TRMC) Test and Evaluation/Science & Technology (T&E/S&T) Program through the U.S. Army Program Executive Office for Simulation, Training and Instrumentation (PEO STRI) under Contract No. W900KK-13-C-0025.

REFERENCES

[1] A. Duel-Hallen, "Fading chanel prediction for mobile radio adaptive transmission systems," *IEEE Proceedings*, vol. 95, Dec. 2007.

[2] S. H. A. Duel-Hallen and H. Hallen, "Long range prediction of fading signals: Enabling adaptive transmission for mobile radio channels," *IEEE Trans. Signal Processing*, vol. 17, May 2000.

[3] A. D. H. T. Eyceoz and H. Hallen, "Deterministic channel modeling and long range prediction of fast fading mobile radio channels," *IEEE Communications Letters*, vol. 2, Sep. 1998.

[4] D. A. M. Sternad, "Channel estimation and prediction for adaptive ofdm downlinks," in *Proc. IEEE Fall Veh. Tech. Conf.*, (Washington, DC), pp. 1283 – 1287, Oct. 2003.

[5] M. V. M. Chen, "Long range channel prediction based on nonstationary parameteric modeling," *IEEE Trans. Signal Processing*, vol. 57, Feb. 1998.

[6] M. Rice, A. Davis, and C. Bettweiser, "Wideband channel model for aeronautical telemetry," *IEEE Trans. Aerospace and Elec. Systems*, vol. 40, pp. 11–11, Jan. 2004.

[7] M. H. Hayes, *Statistical Digital Signal Processing and Modeling*. New York: John Wiley & Sons Inc., 1996.

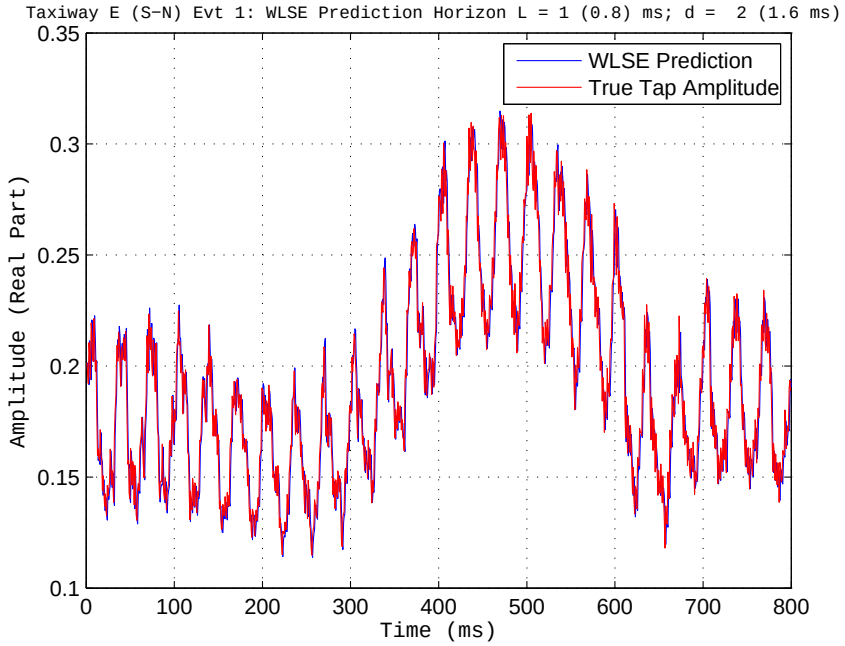

(a) Case 1: Comparison of WLSE predicted versus actual LOS Tap amplitude along the taxiway.

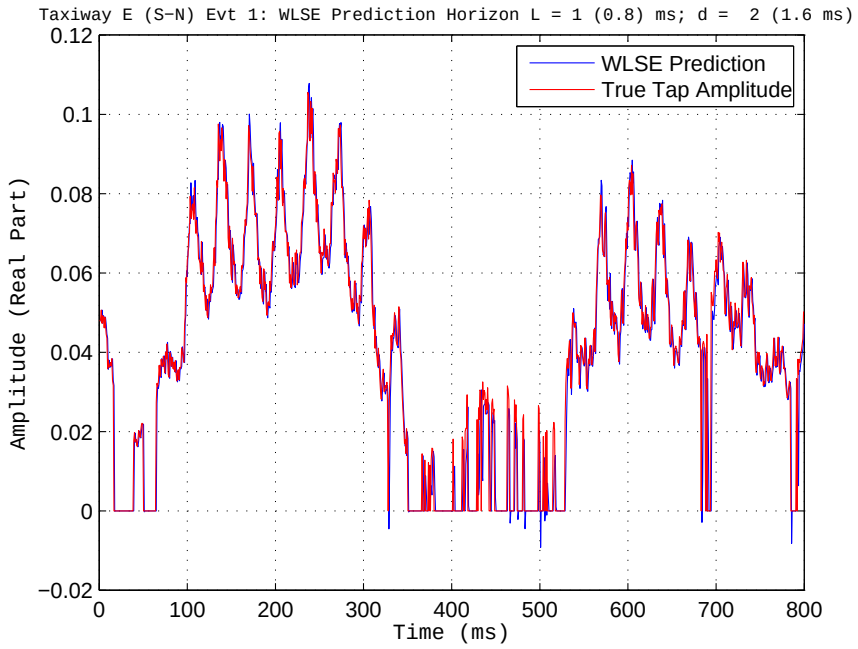

(b) Case 2: Comparison of WLSE predicted versus actual LOS tap amplitude during takeoff.

Figure 1: WLSE LOS tap prediction versus actual LOS channel measurement (Cases 1 and 2 along taxiway). $L = 1$ and $d = 2$.

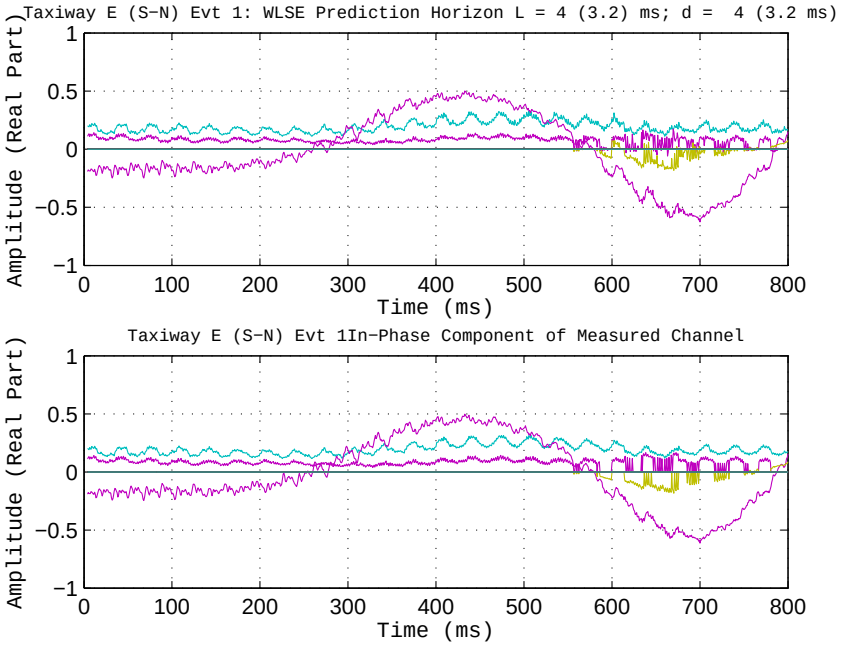

(a) Case 1: Comparison of WLSE predicted versus actual LOS Tap amplitude along the taxiway.

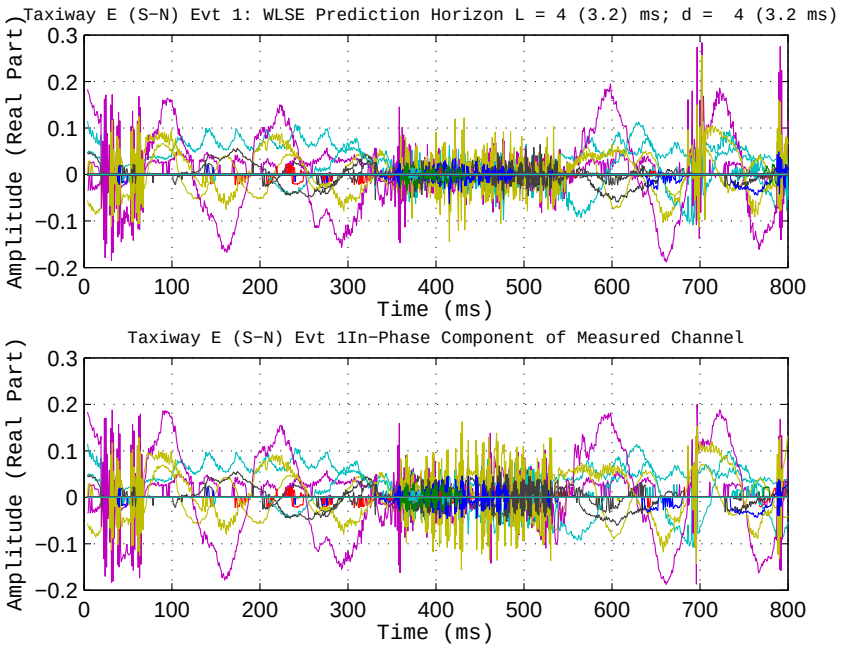

(b) Case 2: Comparison of WLSE predicted versus actual LOS tap amplitude during takeoff.

Figure 2: WLSE prediction of all in-phase taps versus true amplitudes of in-phase channel taps. (Cases 1 and 2 along taxiway). $L = 4$ and $d = 4$.

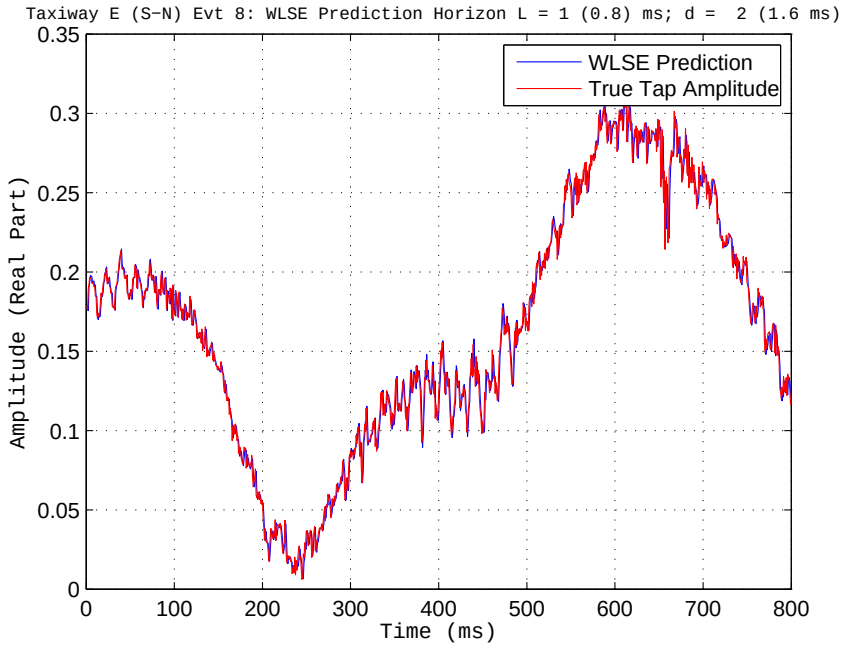

(a) Case 3: Comparison of WLSE predicted versus actual LOS tap amplitude along the taxiway.

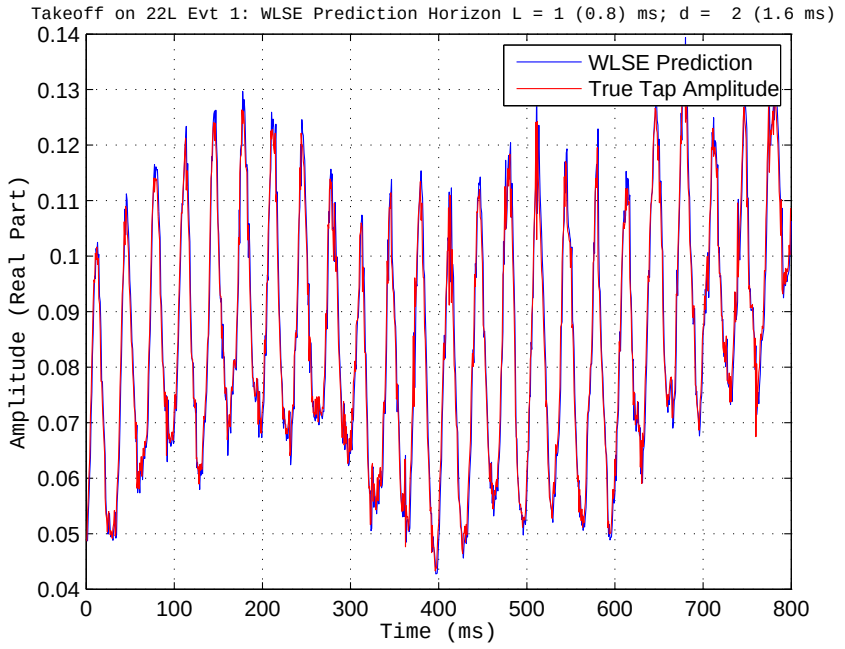

(b) Case 4: Comparison of WLSE predicted versus actual LOS tap amplitude during take-off.

Figure 3: WLSE LOS tap prediction versus actual LOS channel measurement (Cases 3 and 4). $L = 1$ and $d = 2$.

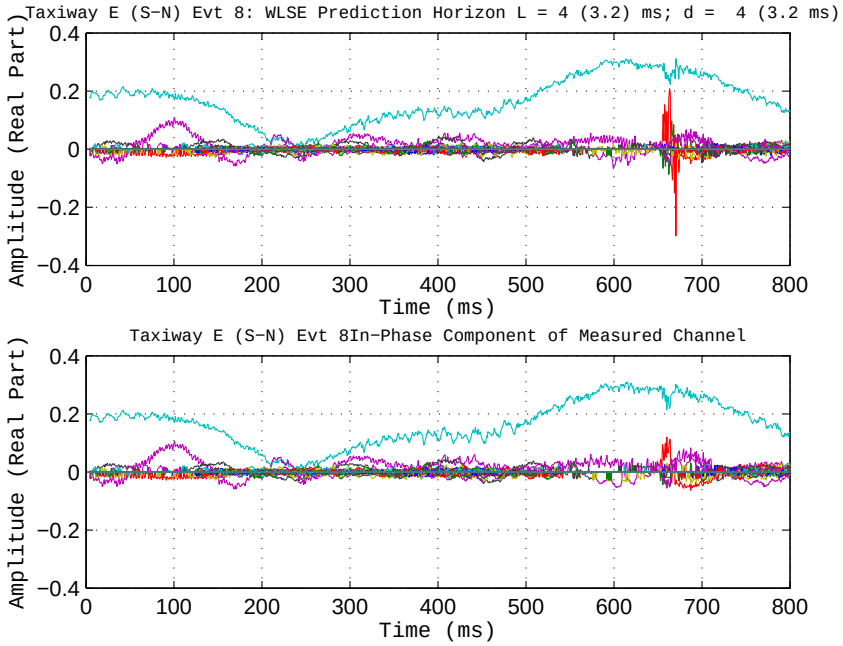

(a) Case 3: Comparison of WLSE predicted versus actual LOS tap amplitude along the taxiway.

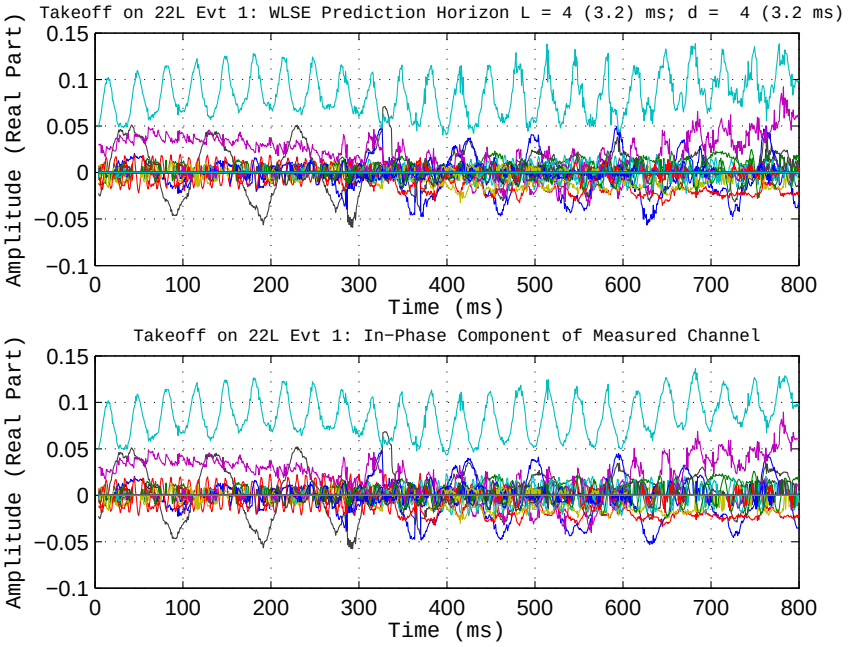

(b) Case 4: Comparison of WLSE predicted versus actual LOS tap amplitude during take-off.

Figure 4: WLSE prediction of all in-phase taps versus true amplitudes of in-phase channel taps. (Cases 3 and 4). $L = 4$ and $d = 4$.

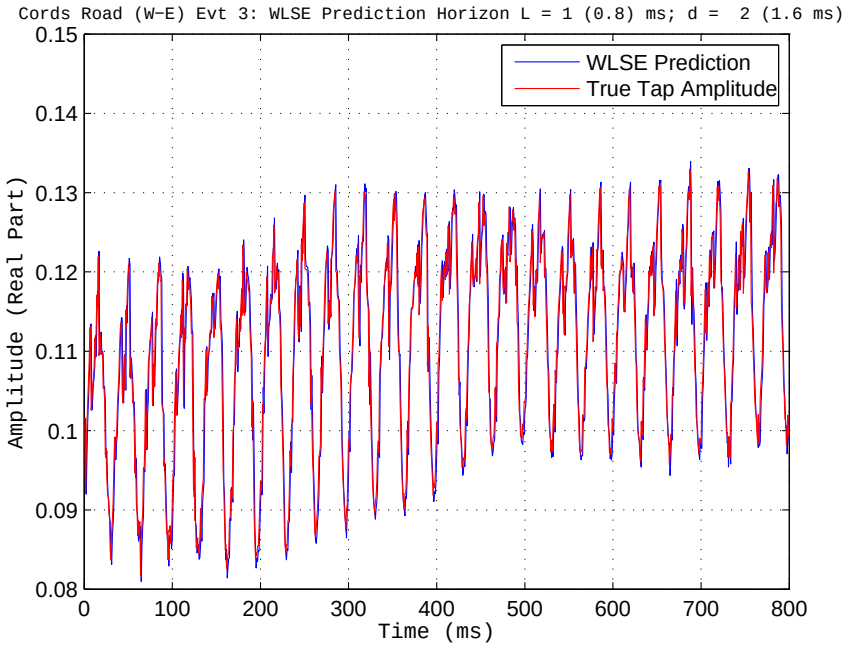

(a) Case 5: Comparison of WLSE predicted versus actual LOS tap amplitude in-flight above Cords Road.

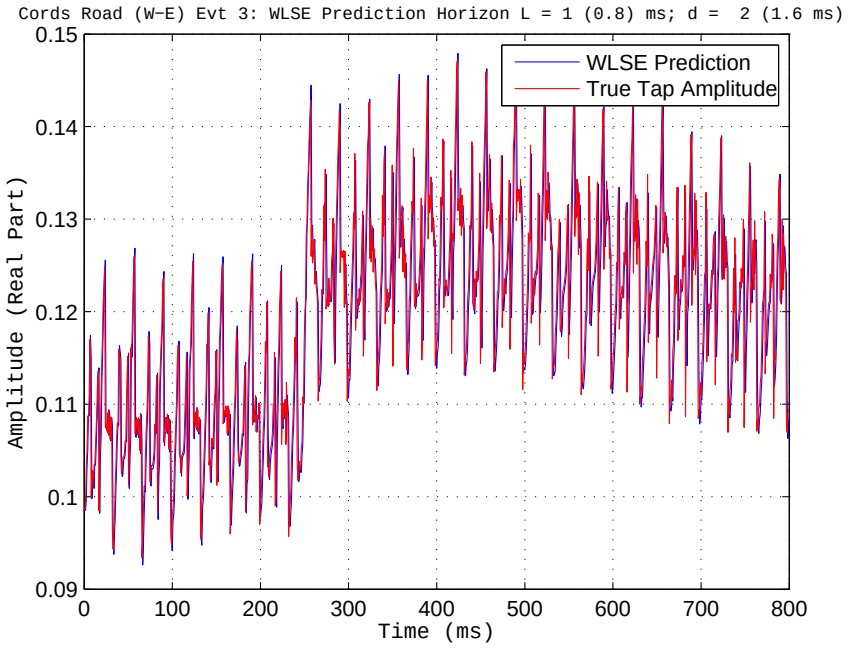

(b) Case 6: Comparison of WLSE predicted versus actual LOS tap amplitude in-flight above Cords Road.

Figure 5: WLSE LOS tap prediction versus actual LOS channel measurement (Cases 5 and 6). $L = 1$ and $d = 2$.

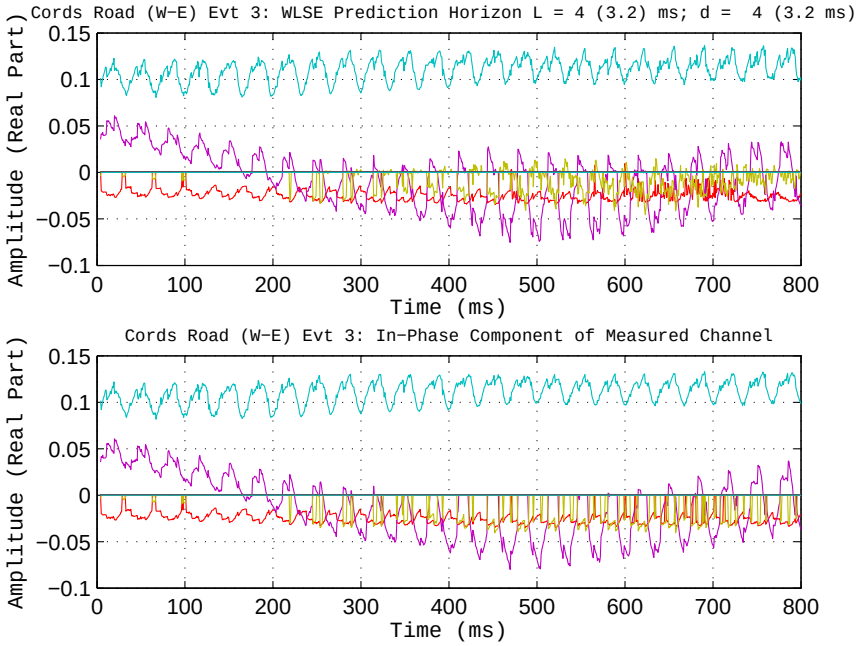

(a) Case 5: Comparison of WLSE predicted versus actual LOS Tap amplitude during flight along Cords Road.

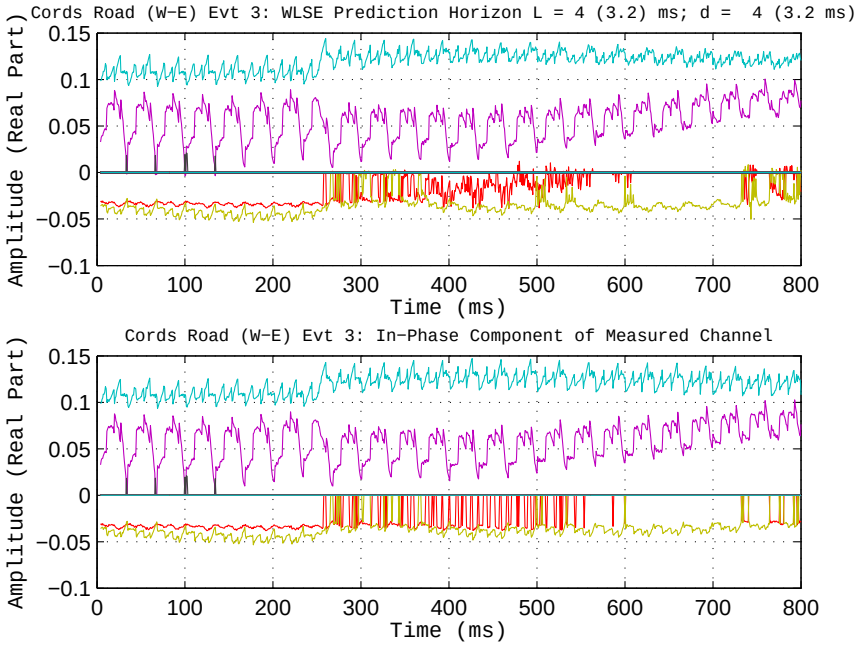

(b) Case 6: Comparison of WLSE predicted versus actual LOS tap amplitude during flight over Black Mountain.

Figure 6: WLSE prediction of all in-phase taps versus true amplitudes of in-phase channel taps. (Cases 5 and 6 while in-flight). $L = 4$ and $d = 4$.

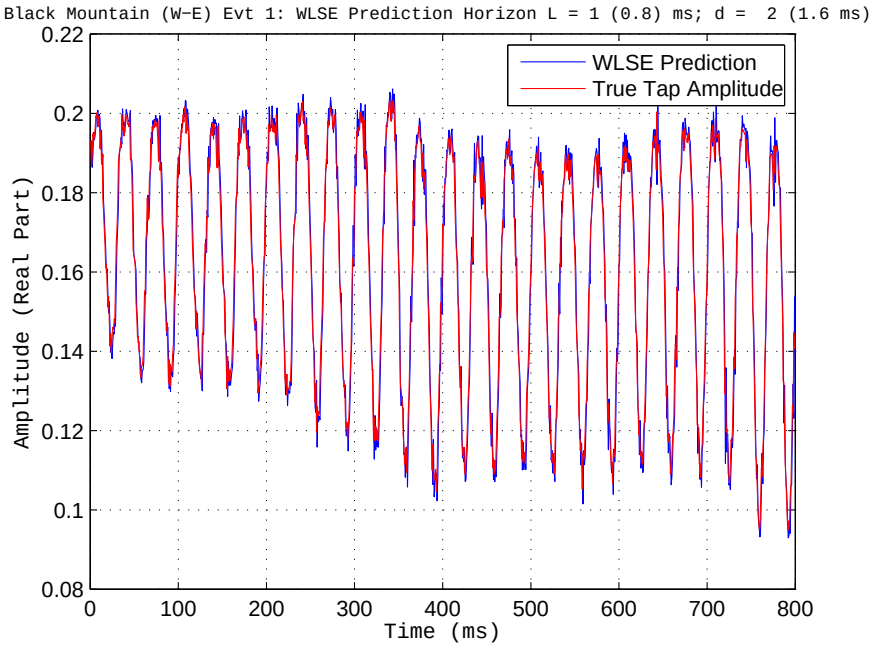

(a) Case 7: Comparison of WLSE predicted versus actual LOS tap amplitude in-flight above Black Mountain.

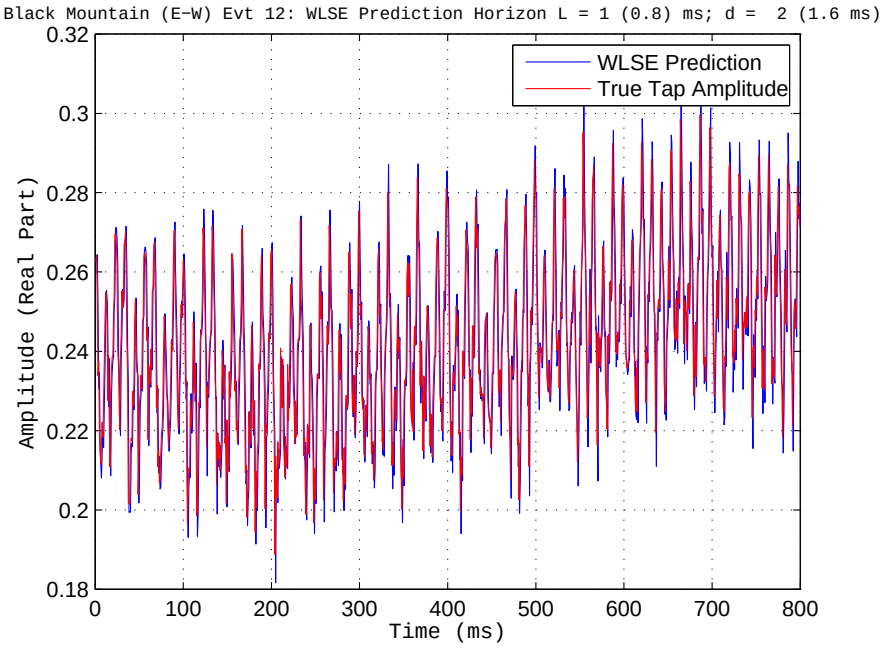

(b) Case 8: Comparison of WLSE predicted versus actual LOS tap amplitude in-flight above Black Mountain.

Figure 7: WLSE LOS tap prediction versus actual LOS channel measurement (Cases 7 and 8). $L = 1$ and $d = 2$.

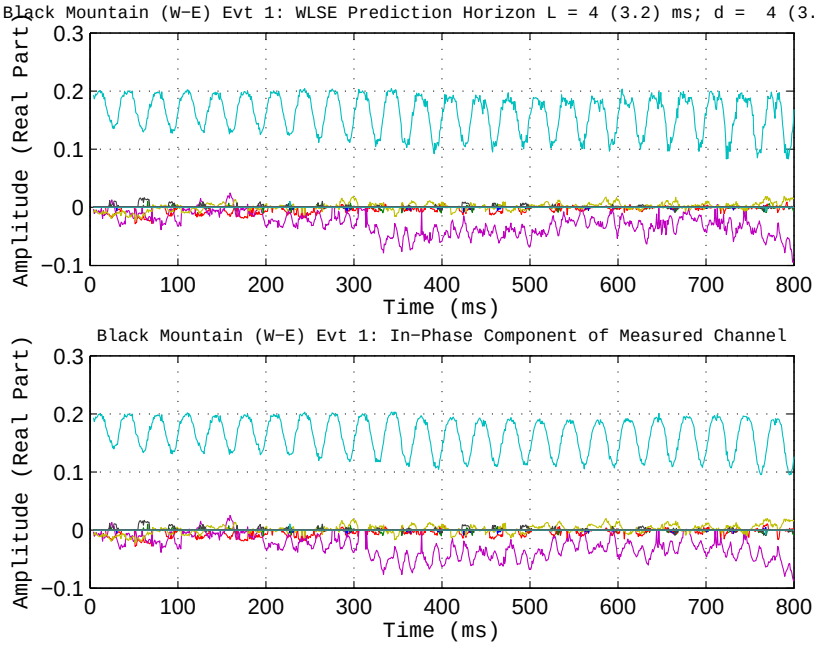

(a) Case 7: Comparison of WLSE predicted versus actual LOS tap amplitude in-flight above Black Mountain.

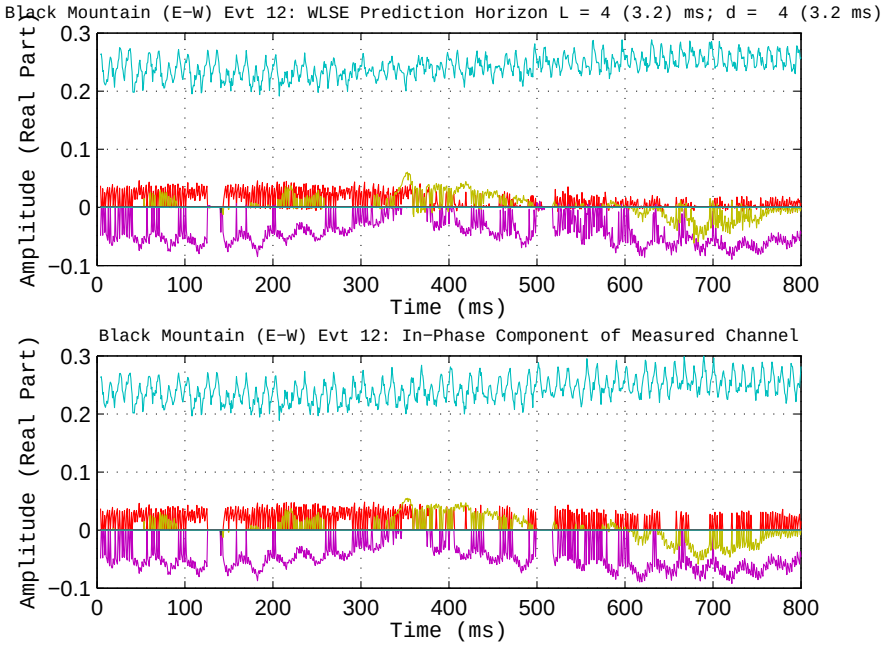

(b) Case 8: Comparison of WLSE predicted versus actual LOS tap amplitude in-flight above Black Mountain.

Figure 8: WLSE prediction of all in-phase taps versus true amplitudes of in-phase channel taps. (Cases 7 and 8 while in-flight). $L = 4$ and $d = 4$.

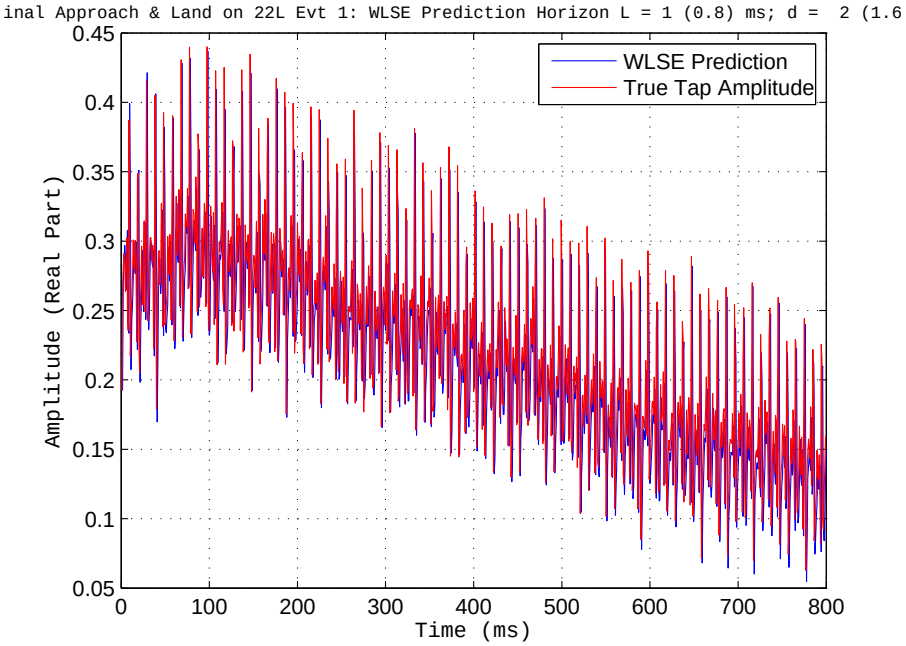

(a) Case 9: Comparison of WLSE predicted versus actual LOS tap amplitude during final approach & landing.

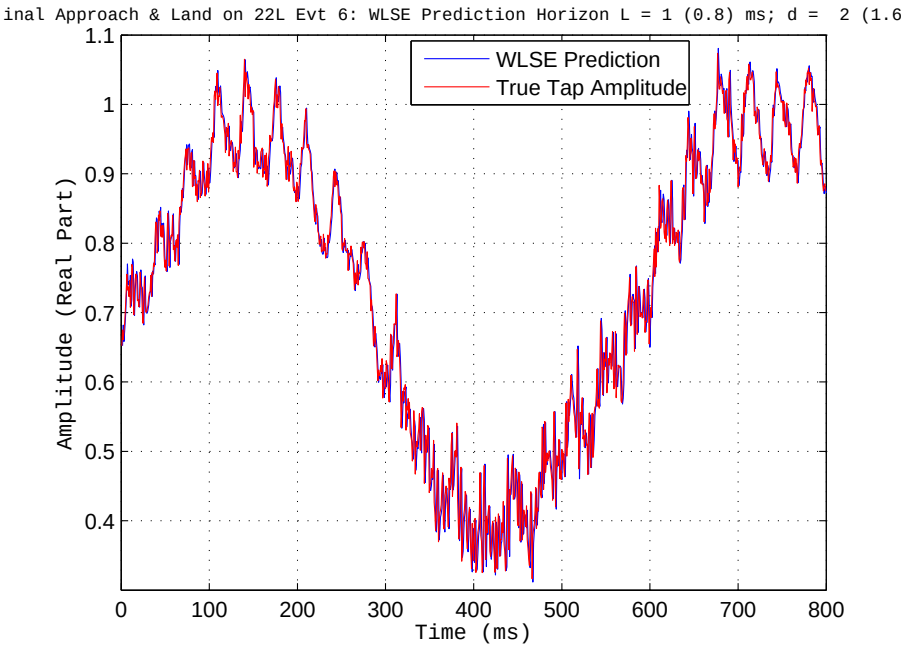

(b) Case 10: Comparison of WLSE predicted versus actual LOS tap amplitude during final approach & landing.

Figure 9: WLSE LOS tap prediction versus actual LOS channel measurement (Cases 9 and 10 during final approach & landing). $L = 1$ and $d = 2$.

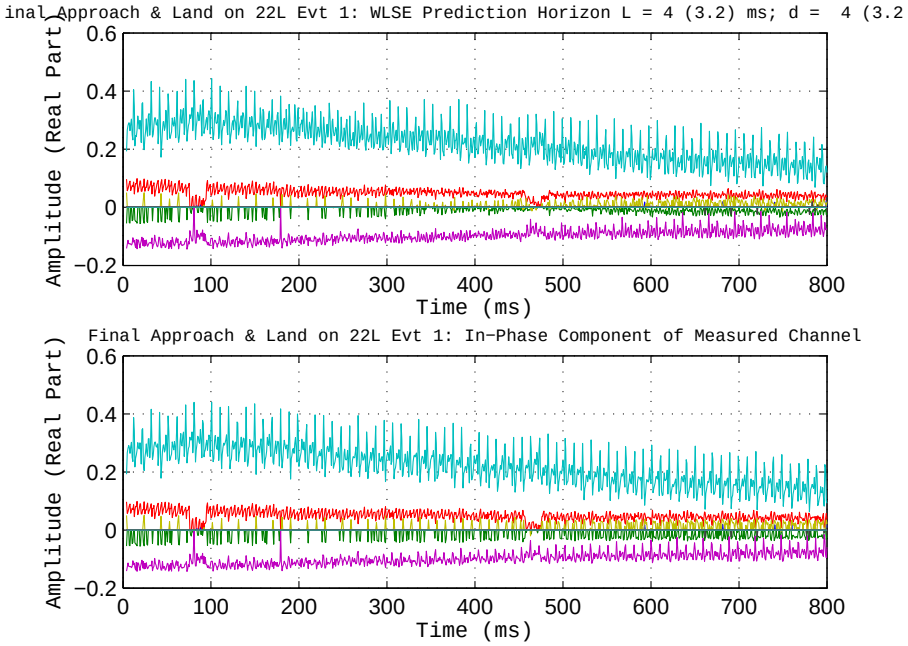

(a) Case 9: Comparison of WLSE predicted versus actual LOS tap amplitude during final approach & landing.

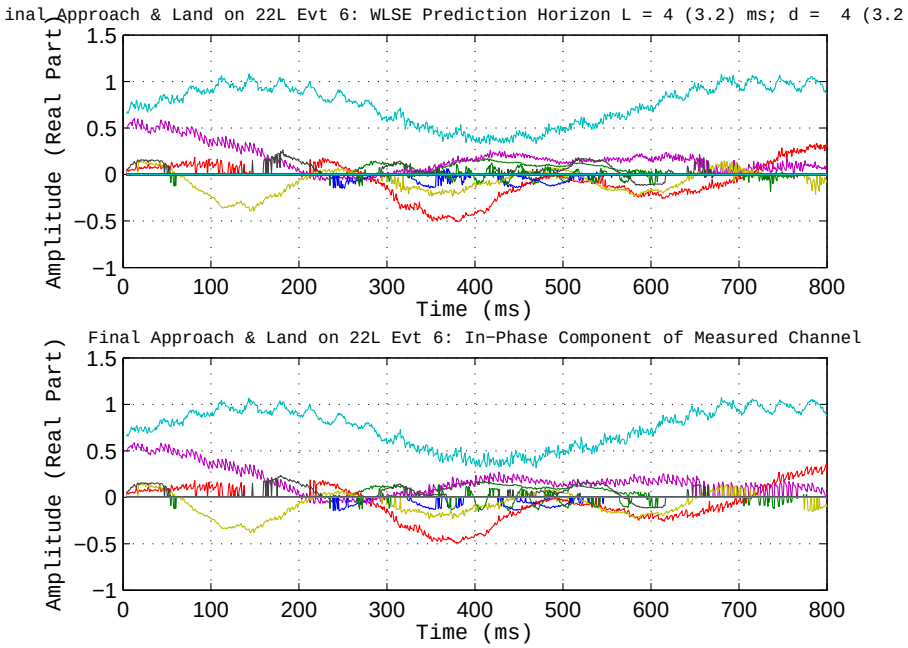

(b) Case 10: Comparison of WLSE predicted versus actual LOS tap amplitude during final approach & landing.

Figure 10: WLSE prediction of all in-phase taps versus true amplitudes of in-phase channel taps. (Cases 7 and 8 while in-flight). $L = 4$ and $d = 4$.